Ideal magnetohydrodynamic flow around a blunt body under anisotropic pressure

Cite as: Physics of Plasmas **7**, 3413 (2000); https://doi.org/10.1063/1.874205
Submitted: 11 November 1999 . Accepted: 07 April 2000 . Published Online: 18 July 2000

Nikolai V. Erkaev, Helfried K. Biernat, and Charles J. Farrugia

Ideal magnetohydrodynamic flow around a blunt body under anisotropic pressure

Nikolai V. Erkaev
Institute of Computational Modelling, Russian Academy of Sciences, Krasnoyarsk, 660036, Russia

Helfried K. Biernat
Space Research Institute, Austrian Academy of Sciences, Lustbühelstraße 46, A-8042 Graz, Austria

Charles J. Farrugia
Institute for the Study of Earth, Oceans, and Space, University of New Hampshire, Durham, New Hampshire 03824

(Received 11 November 1999; accepted 7 April 2000)

The plasma flow past a blunt obstacle in an ideal magnetohydrodynamic (MHD) model is studied, taking into account the tensorial nature of the plasma pressure. Three different closure relations are explored and compared with one another. The first one is the adiabatic model proposed by Chew, Goldberger, and Low. The second closure is based on the mirror instability criterion, while the third depends on an empirical closure equation obtained from observations of solar wind flow past the Earth's magnetosphere. The latter is related with the criterion of the anisotropic ion cyclotron instability. In the presented model, the total pressure, defined as the sum of magnetic pressure and perpendicular plasma pressure, is assumed to be a known function of Cartesian coordinates. The calculation is based on the Newtonian approximation for the total pressure along the obstacle and on a quadratic behavior with distance from the obstacle along the normal direction. Profiles of magnetic field strength and plasma parameters are presented along the stagnation stream line between the shock and obstacle of an ideal plasma flow with anisotropy in thermal pressure and temperature.
 [S1070-664X(00)04407-4]

I. INTRODUCTION

The problem of supersonic flow of a magnetized plasma around blunt bodies is substantially different from that of pure gasdynamics if the plasma is highly conducting. This is because magnetic forces give rise to an asymmetric three-dimensional flow pattern. The structure of an ideal magnetohydrodynamic (MHD) flow around obstacles has special features caused by the ''frozen-in'' magnetic field, even though this field is relatively small in the flow upstream of the bow shock. During the last three decades substantial advances have been made in solving the MHD flow problem. Spreiter *et al.*[1] used MHD modeling in the kinematic approximation for the magnetic field. In their approach, the plasma parameters were obtained from gasdynamics, and using the flow field thus derived, the magnetic field is obtained from the equations of magnetic flux conservation and magnetic induction. However, the magnetic field calculated in the kinematic approximation has a strong singularity at the surface of the obstacle. This implies that the magnetic field has a strong influence on the flow in a thin boundary layer near the surface of the obstacle. To deal with this problem, a boundary layer technique was developed by Zwan and Wolf,[2] Erkaev,[3] Erkaev and Mezentsev,[4] Erkaev *et al.*,[5] and others. This boundary layer, where the magnetic pressure dominates over the plasma pressure, is called the magnetic barrier or plasma depletion layer. The latter emphasizes the systematic decrease of plasma density which accompanies the magnetic field pileup.

In parallel, results of the global MHD simulations of a plasma flow around blunt bodies (sphere and ellipsoid) appeared.[6,7] These simulations give quite good descriptions of the detached shock wave and the large scale features of MHD flow around the blunt body. However, a global model cannot properly describe features in relatively small-scale layers such as the magnetic barrier.

Further developments of MHD flow models were related with the anisotropy of plasma pressure in a magnetized plasma.[8,9] Taking the pressure anisotropy into account, we have two pressure components, one perpendicular and one along the magnetic field, instead of one in the isotropic case. Since we have more parameters to be calculated, we need an additional equation which determines the relation between the two pressures. This equation is required to complete the anisotropic MHD equation system.

The aim of this paper is to analyze the behavior of the magnetic field and plasma parameters of an ideal MHD flow past a blunt obstacle under different relations between perpendicular and parallel pressures which have been proposed. Comparison of results has potential data analysis applications.

II. BRIEF THEORETICAL SURVEY

The theory of Chew, Goldberger, and Low[10] proposes the expression for the tensor of plasma pressure in a magnetized collisionless plasma,

$$P_{i,k}=p_{\perp}\delta_{i,k}+(p_{\parallel}-p_{\perp})B_iB_k/B^2. \tag{1}$$

Here, we use the symbols $\perp$ and $\parallel$ to denote quantities perpendicular and parallel to the magnetic field, respectively. In this theory, the components of pressure tensor are determined by two expressions which are called the double-adiabatic equations,

$$\frac{d}{dt}\left(\frac{p_\perp}{\rho B}\right)=0, \quad \frac{d}{dt}\left(\frac{p_\parallel B^2}{\rho^3}\right)=0. \tag{2}$$

Using these expressions together with MHD equations of magnetic induction, conservation of momentum, mass, and magnetic flux, one can get a self-consistent anisotropic MHD model.

Anisotropic plasma described by this double-adiabatic MHD model has two MHD instabilities[11] which depend on the relation between the components $p_\perp$ and $p_\parallel$. The first one is the ''fire hose'' instability which occurs when $p_\parallel - p_\perp > B^2/(4\pi)$. The second one is mirror instability which occurs for sufficiently large ratio of perpendicular and parallel pressures: $p_\perp/p_\parallel > 6(1+B^2/(8\pi p_\perp))$. Here, the factor of 6 in the right side of this relation appears only in the (inadequate) MHD treatment of the mirror instability. This factor is absent in the more correct criterion of the mirror instability derived in the kinetic description,[12]

$$p_\perp/p_\parallel > (1+B^2/(8\pi p_\perp)). \tag{3}$$

In the kinetic description we also have the proton cyclotron anisotropy instability,[13] which is more important in the region of low plasma beta (beta is the ratio of plasma pressure and magnetic pressure). Thus, these two instabilities are the main physical factors which bound the ratio of pressures $p_\perp/p_\parallel$.

In addition, there are two empirical approaches to determine the ratio of perpendicular and parallel temperatures as a function of other plasma parameters. These approaches are based on observations of the solar wind flow about the Earth's magnetosphere.

The first approach proposed by Hau *et al.*[14] is a modification of the double-adiabatic equations[10] with empirical polytrope exponents,

$$\frac{d}{dt}\left(\frac{p_\perp}{\rho B^{\gamma_1-1}}\right)=0, \quad \frac{d}{dt}\left(\frac{p_\parallel B^{\gamma_2-1}}{\rho^{\gamma_2}}\right)=0. \tag{4}$$

As the authors[14] point out, in space physics these empirical exponents obtained from data vary from event to event in the ranges $0.74<\gamma_1<1.17$, and $0.9<\gamma_2<1.47$ for protons.

The second approach proposed by Gary *et al.*[15] and Denton *et al.*[16] is to use an empirical relation between the ratio of perpendicular and parallel plasma pressures and parallel plasma beta as a closure equation for the MHD system,

$$p_\perp/p_\parallel > 1+0.847(B^2/(8\pi p_\parallel))^{0.48}. \tag{5}$$

This relation is based on an analysis of magnetosheath data returned by the Composition Charge Explorer (CCE) on the Active Magnetospheric Particle Trace Explorer (AMPTE) mission in the 1980's. This anticorrelation between anisotropy and parallel plasma beta parameter obtained from observations is similar to that for the threshold of the proton cyclotron instability.[17]

In the work by Erkaev *et al.*,[9] the empirical relation as given above, (5), is used. In this study, we generalize this work by investigating the implications for MHD flow model of each of three closure relations: double-adiabatic equations (2), mirror (3), and empirical (5) to complete the system of MHD equations.

III. BASIC EQUATIONS: STATEMENT OF PROBLEM

We work with the system of MHD equations for an infinitely conducting, inviscid, dissipationless fluid, i.e.,

$$\rho(\mathbf{u}\cdot\nabla)\mathbf{u}+\nabla\cdot\mathbf{P}+\frac{1}{8\pi}\nabla B^2-\frac{1}{4\pi}(\mathbf{B}\cdot\nabla)\mathbf{B}=0, \tag{6}$$

$$\nabla\cdot\left(\rho\mathbf{u}\left(u^2/2+\frac{1}{4\pi}B^2/\rho+\mathcal{E}\right)+\mathbf{P}\cdot\mathbf{u}-\frac{1}{4\pi}(\mathbf{B}\cdot\mathbf{u})\mathbf{B}\right)=0, \tag{7}$$

$$\nabla\cdot(\rho\mathbf{u})=0, \quad \nabla\times(\mathbf{u}\times\mathbf{B})=0, \quad \nabla\cdot\mathbf{B}=0. \tag{8}$$

Here, ρ, $\mathbf{u}$, and $\mathbf{B}$ are the mass density, velocity, and magnetic field, respectively. Quantity $\mathbf{P}$ is the pressure tensor $P_{ik}=p_\perp\delta_{ik}+(p_\parallel-p_\perp)B_iB_k/B^2$ and $\mathcal{E}$ is the thermal energy: $\mathcal{E}=p_\perp/\rho+0.5p_\parallel/\rho$. Equation (6) is the momentum equation; Eq. (7) expresses the conservation of energy flux, while Eqs. (8) are the mass continuity equation, the frozen-in magnetic field relation, and the divergenceless condition of the magnetic field, respectively. In the general case, we can consider the relation between perpendicular and parallel pressures in the following fashion:

$$p_\perp=p_\parallel F(\rho,B,p_\parallel). \tag{9}$$

In the particular cases this function is given as follows:

(1) Isotropic MHD model: $F=1$.
(2) Anisotropic adiabatic model: $F=\text{const}\,B^3/\rho^2$.
(3) Criterion of the mirror instability: $F=0.5(1+\sqrt{1+4/\beta_\parallel})$, where $\beta_\parallel$ is the ratio of the parallel plasma pressure and magnetic pressure: $\beta_\parallel=8\pi p_\parallel/B^2$.
(4) Empirical relation: $F=1+A/\sqrt{\beta_\parallel}$, $A=0.848$.

In our study, we use the closure relations formulated above only for the magnetosheath region. They are not expected to be valid through the shock structure.

For a supersonic and superalfvénic flow, a detached bow shock forms upstream of obstacle separating the unperturbed (and assumed uniform) flow from the thermalized medium downstream. At the bow shock we satisfy as boundary conditions the isotropic MHD Rankine–Hugoniot jump relations,[18] i.e.,

$$\begin{aligned}
&[\rho u_n^2+\Pi]=0,\\
&\left[\rho u_n\mathbf{u}_t-\frac{B_n}{4\pi}\mathbf{B}_t\right]=0,\\
&[\rho u_n]=0, \quad [B_n]=0,\\
&[(\mathbf{u}\times\mathbf{B})_t]=0,\\
&\left[\rho u_n\left(\frac{u^2}{2}+\left(\frac{5}{2}\right)\frac{p}{\rho}\right)+\frac{u_nB^2-B_n(\mathbf{u}\cdot\mathbf{B})}{4\pi}\right]=0.
\end{aligned} \tag{10}$$

In (10), $\Pi = p + B^2/8\pi$, and the subscripts n and t represent quantities normal and tangential to the bow shock, respectively. $[Q]$ denotes the jump of Q across the shock. Equations (10) are the conservation expressions for (from top to bottom) the momentum normal to the bow shock; the tangential momentum; the mass flux; the normal field component; the tangential electric field; and, finally, the total energy. We also impose the no-flow condition: $u_n = 0$ at the surface of the obstacle assumed to be impermeable for the plasma.

In our model, the obstacle is a paraboloid of revolution, $x = L_0 - (y^2+z^2)/(2L_0)$, with L_0 the radius of curvature at the stagnation point. The geometry of the problem is shown in Fig. 1. The magnetic field vector upstream of the shock points in the z direction and is orthogonal to the flow velocity, $\mathbf{u}_\infty$, which is along $-x$. The body-centered coordinate system (l,μ,ϕ) is defined such that l is the distance along a generator, μ is the distance from the obstacle along its normal, and ϕ is the azimuthal angle. Parameter $r(l)$ denotes the distance of a given point on the surface of the obstacle from the symmetry axis.

We seek a solution of the ideal MHD equations corresponding to the given parameters of an upstream, uniform medium and satisfying the boundary conditions at the shock front and at the surface of the obstacle. We first introduce dimensionless variables as follows:

$$\mathbf{R} = \frac{\tilde{\mathbf{R}}}{L_0}, \quad P = \frac{\tilde{P}}{\rho_\infty u_\infty^2}, \quad \mathbf{B} = \frac{\tilde{\mathbf{B}}}{B_\infty}, \quad \mathbf{u} = \frac{\tilde{\mathbf{u}}}{u_\infty},$$

where $\mathbf{R} = (x,y,z)$. In steady state, the dimensionless MHD equations are then

$$\begin{aligned}
&\rho(\mathbf{u}\cdot\nabla)\mathbf{u} + \nabla\Pi - \epsilon(\mathbf{B}\cdot\nabla)((1+\alpha)\mathbf{B}) = 0,\\
&\nabla\cdot(\rho\mathbf{u}) = 0, \quad \nabla\times(\mathbf{u}\times\mathbf{B}) = 0, \quad \nabla\cdot\mathbf{B} = 0,\\
&\nabla\cdot[\rho\mathbf{u}(u^2/2 + 2P_\perp/\rho + 0.5P_\parallel/\rho + \epsilon B^2/\rho)\\
&\qquad -(1+\alpha)\mathbf{B}(\mathbf{u}\cdot\mathbf{B})] = 0,\\
&\alpha = (P_\perp - P_\parallel)/(\epsilon B^2), \quad \Pi = p_\perp + \epsilon B^2/2.
\end{aligned} \tag{11}$$

Parameter ϵ is the inverse square of the upstream Alfvén Mach number, $\epsilon = B_\infty^2/(4\pi\rho_\infty u_\infty^2)$.

IV. MAGNETIC STRING EQUATIONS

To describe an ideally conducting plasma, we use material coordinates (ξ,η,τ). A given streamline is described by a pair (ξ,η), while parameter τ varies along the streamline and gives the Lagrangian time. In the steady state, these coordinates may be introduced by means of the equations

$$(\mathbf{u}\cdot\nabla)\xi = 0, \quad (\mathbf{u}\cdot\nabla)\eta = 0, \quad (\mathbf{u}\cdot\nabla)\tau = 1. \tag{12}$$

These coordinates can be chosen to be proportional to Cartesian coordinates in the unperturbed, upstream flow,

$$\xi = z, \quad \eta = y, \quad \tau = -x. \tag{13}$$

In this case, variables η and τ are constant along magnetic field lines everywhere. Similar coordinates called ''frozen-in coordinates,'' were introduced by Pudovkin and Semenov.[19]

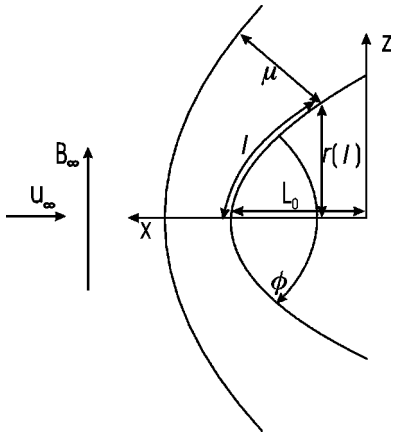

FIG. 1. Schematic illustrating the geometry of the problem. The x axis points from the Earth to the Sun; the magnetic field direction upstream of the bow shock defines the z axis, with the y axis completing the right-handed set (x,y,z). The system (l,μ,ϕ) is the body-centered coordinate system in which the ideal MHD equations are expressed before numerical integration.

In frozen-in coordinates, the nondissipative MHD equations can be written as follows:

$$\left(\frac{\partial^2\mathbf{R}}{\partial\tau^2} - \epsilon\frac{\partial}{\partial\xi}\left(\rho(1+\alpha)\frac{\partial\mathbf{R}}{\partial\xi}\right)\right)_i + \frac{D(\Pi,R_j,R_k)}{D(\xi,\eta,\tau)} = 0, \tag{14}$$

$$\alpha = (p_\perp - p_\parallel)/(\epsilon B^2),$$

$$p_\perp + \epsilon\frac{\rho^2}{2}\left(\frac{\partial\mathbf{R}}{\partial\xi}\right)^2 = \Pi, \tag{15}$$

$$\frac{\partial}{\partial\tau}(u^2/2 + \epsilon B^2/\rho + 2p_\perp/\rho + 0.5p_\parallel/\rho) = \epsilon\frac{\partial}{\partial\xi}((1+\alpha)\mathbf{u}\cdot\mathbf{B}), \tag{16}$$

$$\mathbf{u} = \frac{\partial\mathbf{R}}{\partial\gamma}, \quad \mathbf{B} = \rho\frac{\partial\mathbf{R}}{\partial\alpha}, \tag{17}$$

$$\frac{D(x,y,z)}{D(\xi,\eta,\tau)} = \frac{1}{\rho}. \tag{18}$$

Here, the triplet (i,j,k) stands for a cyclic permutation of (1, 2, 3); α is the anisotropy parameter; and $D(\ldots)/D(\ldots)$ is the Jacobian of the transformation. Equation (14) is the ith component of the momentum equation. Equation (15) is an expression for the total perpendicular pressure. Equation (16) is the energy equation, and Eq. (18) expresses the conservation of mass.

We next make two simplifying assumptions on the behavior of the total pressure Π between the shock and the obstacle. In our method, its variation along the normal to the surface of the obstacle is prescribed. Specifically, we assume a quadratic dependence,

$$\Pi = \Pi_m\left(1 - \frac{\mu^2}{\delta^2}\right) + \Pi_s\frac{\mu^2}{\delta^2}, \tag{19}$$

where Π_m and Π_s are the values of the total perpendicular pressures at the surface of the obstacle, and immediately downstream of the detached shock (with $\Pi_m > \Pi_s$), respectively, and δ is the distance from the obstacle to the shock

along the normal. The coefficients, Π_m and Π_s, are determined from the boundary conditions at the obstacle and detached shock. Along the obstacle, Π obeys the Newtonian formula with its $\cos^2\theta$ dependence on the angle θ between the normal to the surface of the obstacle and the X axis

$$\Pi_m=(\Pi_0-\Pi_\infty)\cos^2\theta+\Pi_\infty, \tag{20}$$

where Π_0 is the total pressure at the stagnation point of obstacle. This formula is well-known in gasdynamics as a good analytical approximation for the pressure on a streamlined obstacle. The latter two assumptions are the same as those we used in the isotropic case.[5,20–22]

A further point is the following. Since we do not solve a full set of MHD equations because we replace the momentum equation in the direction normal to the surface of the obstacle by the condition (19) on the total pressure Π, it is not *a priori* evident that the entropy equation will be satisfied. We have carried out a consistency check and found that the quadratic variation is consistent with entropy conservation along the stagnation streamline in the case of isotropic pressure.

The final step before integrating numerically is to express the functions $x(\xi,\eta,\tau)$, $y(\xi,\eta,\tau)$, $z(\xi,\eta,\tau)$ in terms of the body coordinates (μ,l,ϕ) of Fig. 1. The transformed set of equations is as follows:

$$\frac{\partial u_l}{\partial\gamma}-\epsilon\frac{\partial(1+\alpha)B_l}{\partial\xi}+\frac{1}{\rho(1+K\mu)}\frac{\partial\Pi(l,\mu)}{\partial l}=F_l, \tag{21}$$

$$\frac{\partial u_\phi}{\partial\gamma}-\epsilon\frac{\partial(1+\alpha)B_\phi}{\partial\xi}=F_\phi, \tag{22}$$

$$p_\perp+\epsilon\tfrac{1}{2}(B_l^2+B_\phi^2+B_\mu^2)=\Pi(l,\mu), \tag{23}$$

$$\frac{\partial}{\partial\gamma}(u^2/2+\epsilon B^2/\rho+2P_\perp/\rho+0.5P_\parallel/\rho)$$

$$=\epsilon\frac{\partial}{\partial\xi}((1+\alpha)(u_lB_l+u_\mu B_\mu+u_\phi B_\phi)), \tag{24}$$

$$u^2=u_l^2+u_\phi^2+u_\mu^2,\quad B^2=B_l^2+B_\phi^2+B_\mu^2, \tag{25}$$

$$u_l=(1+K\mu)\frac{\partial l}{\partial\tau},\quad B_l=\rho(1+K\mu)\frac{\partial l}{\partial\xi}, \tag{26}$$

$$u_\phi=(r+\mu\sqrt{1-r_l^2})\frac{\partial\phi}{\partial\tau},\quad B_\phi=\rho(r+\mu\sqrt{1-r_l^2})\frac{\partial\phi}{\partial\xi}, \tag{27}$$

$$u_\mu=\frac{\partial\mu}{\partial\tau},\quad B_\mu=\rho\frac{\partial\mu}{\partial\xi}, \tag{28}$$

$$\frac{D(l,\mu,\phi)}{D(\xi,\eta,\tau)}(1+K\mu)(r+\sqrt{1-r_l^2})=\frac{1}{\rho}. \tag{29}$$

F_l and F_ϕ are expressions depending on l, ϕ, μ, u_l, u_ϕ, u_μ, B_l, B_ϕ, B_μ; K is the local curvature of the obstacle, and is a function of l; r, which is the distance from a given point on the obstacle to the stagnation line, is a known function of l; and r_l denotes the derivative dr/dl. With Π prescribed as above, Eqs. (21)–(28) no longer contain derivatives with respect to η. The system (21)–(28) thus represents a 2D, hyperbolic set of equations.

The shock front is taken to be a hyperboloid parametrized by the three quantities q, L_1, and d,

$$x=L_1(-q\sqrt{1+z^2/(qL_1^2)+y^2/(qL_1^2)}+q)+d+L_0,$$

where L_1 is the radius of curvature of the shock front at the subsolar point, q is a cotangent squared of the cone angle at infinity, and d is the shock stand-off distance (i.e., the subsolar thickness of the magnetosheath). The cone angle is assumed to be equal to the Mach cone angle.

The magnetosheath parameters are finally obtained iteratively as follows. We first apply the jump conditions (10) on the input parameters at an initial bow shock whose L_1 and d parameters are obtained from gasdynamics. This gives plasma and magnetic field quantities just downstream of the bow shock. In this first step, we assume $p_\parallel=p_\perp$ just downstream of the bow shock, but in subsequent steps we evolve the pressures according to the suitable closure relation (9). In our study, we consider the four different cases: double-adiabatic model, criterion of the mirror instability, empirical relation, and isotropic MHD model.

We should note that the influence of temperature anisotropy on the jump conditions of plasma parameters on the fast shock is an additional problem which is beyond the scope of this paper. Applying the closure relation of the bounded anisotropy models just downstream of the shock, we might slightly overestimate the effect of anisotropy on plasma parameters. But, this overestimation is small in a case of large Mach numbers as considered in our paper.

We use a finite difference Lax–Wendroff scheme to integrate Eqs. (21) to (28) from the shock to the obstacle, and thus obtain functions $l(\xi,\eta,\tau)$ and $\phi(\xi,\eta,\tau)$, as well as the components of the velocity (u_l,u_ϕ) and the magnetic field (B_l,B_ϕ) in a direction tangential to the surface of the obstacle. When we integrate for the first time, we assume $\mu=0$ in (21)–(28), which corresponds to thin boundary layer equations.[4] The function $\mu(\xi,\eta,\tau)$ is then obtained from the Jacobian equation (29) by the method of characteristics. (The characteristics for this equation correspond to the normal to the surface of the obstacle.) We integrate (28) and (29) in the reverse direction, i.e., from the obstacle (where $\mu=0$) to the bow shock to obtain magnetosheath quantities normal to the obstacle.

The numerical solution obtained in a first run gives a new estimate of the distance μ between the obstacle and the detached shock along any given normal. This will generally differ from our first estimate. The code is then rerun and the first estimate is improved.

V. RESULTS

Figure 2 shows, from top to bottom, profiles along the stagnation streamline of the density, perpendicular and parallel plasma (proton) pressures obtained for different closure relations: isotropic model, mirror criterion, empirical criterion, and the double-adiabatic model. The pressure is normalized to the dynamic pressure of the flow: $P_{d\infty}=\rho_\infty u_\infty^2$.

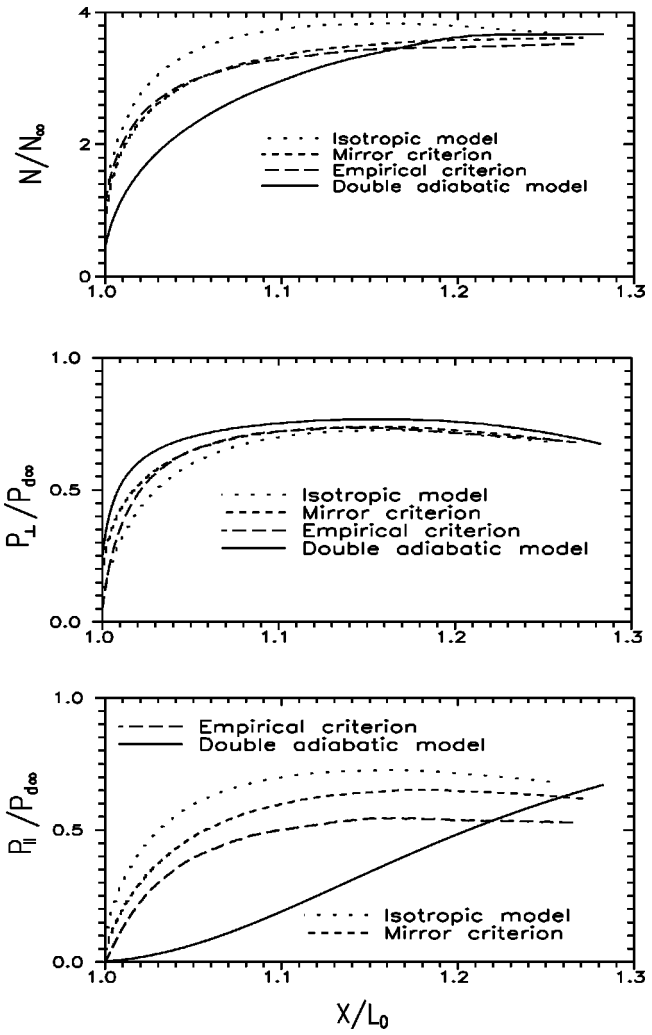

FIG. 2. Variation of plasma density and perpendicular and parallel pressures. Distances in the magnetosheath are normalized to the radius of curvature of the obstacle at the stagnation point, L_0. All curves are shown from the bow shock (at right) to the obstacle. Profiles for the isotropic limit are shown with short dashes.

The upstream sonic and Alfvén Mach numbers are $M_{s\infty} = M_{A\infty} = 10$. The distance x is normalized to the radius of curvature determined at the stagnation point of the obstacle. The origin of the Cartesian coordinates x, y, z coincides with the center of curvature of the obstacle related to the stagnation point. The corresponding profiles for isotropic plasma are included for comparison and are shown by the dotted lines.

The first panel shows that across the isotropic magnetosheath, the density goes through a broad, shallow maximum before it decreases, at first slowly, and then steeply toward the obstacle. This behavior is qualitatively similar to that obtained in isotropic 3D MHD simulations by Wu[6] in most of the part of the region between the shock and obstacle. The difference is essential only in the vicinity of the obstacle, where the density obtained in our solution decreases to a much smaller value. This feature is also in agreement with the semianalytical result of Zwan and Wolf[2] obtained for an isotropic plasma.

Anisotropy brings about an additional decrease of density in all three models. In the anisotropic models, the density is monotonically decreasing throughout the region between the shock and the obstacle. In the double-adiabatic model, anisotropy is not bounded and thus all effects of anisotropy are much more pronounced than in the other cases.

The profiles of the perpendicular pressure are shown on the second panel. In this panel, the value of the pressure is lowest for the isotropic case. The largest is the perpendicular pressure obtained from the double-adiabatic model. The profiles of perpendicular pressure for the models with the mirror instability criterion (3) and empirical criterion (5) are close to each other throughout most of the part of the trajectory between the shock and the obstacle. But just near the obstacle the perpendicular pressure in the mirror-bounded model is essentially bigger than that in the model with the empirical criterion. This is because the beta is very low in the depletion layer near the obstacle, and the mirror mode allows larger anisotropy at low beta as shown by Gary *et al.*[17]

The profiles of the parallel pressure shown on the third panel are in reversed order compared to those of the perpendicular pressures. The profile corresponding to the double-adiabatic model has a position below the others. Throughout the line between the shock and the obstacle, the parallel pressure's obtained, assuming isotropy is the largest. The profiles of parallel pressure for the models with mirror and empirical criterions lie between those for the double-adiabatic and isotropic models. The parallel pressure for the model with mirror criterion exceeds the parallel pressure for the model with the empirical criterion throughout the whole region between the detached shock and the obstacle. Comparing panels 2 and 3, we see that quite generally, anisotropy leads to an increase of the perpendicular pressure and decrease of the parallel pressure. Since $p_\parallel$ is less than $p_\perp$, energy exchange has a greater effect on $p_\parallel$.

Figure 3 shows the variation along the stagnation streamline of the temperatures perpendicular and parallel to the magnetic field, and the temperature ratio $T_\perp / T_\parallel$ from the detached shock (right) to the obstacle. The first panel shows variations of perpendicular temperature for the different models. One can see that the behavior of the perpendicular temperature of the double-adiabatic model is completely different from that related to the other models. In accordance with the first adiabatic law, $T_\perp$ is proportional to B, and thus it increases monotonically from the shock to the obstacle. The temperature obtained for the model with the mirror criterion also increases, but its variation is rather small. Variation of temperatures related to the model with the empirical criterion has a shallow maximum. This temperature is very close to that for the mirror criterion model in the region between the maximum point and the shock. But, the difference becomes rather big near the obstacle where the temperature goes down for the model with the empirical criterion. This is like the observations reported by, e.g., Phan *et al.*[23]

The second panel shows variations of parallel temperature between the shock and the obstacle. The parallel temperature related to the double-adiabatic case decreases monotonically from the shock to the obstacle. It is much lower

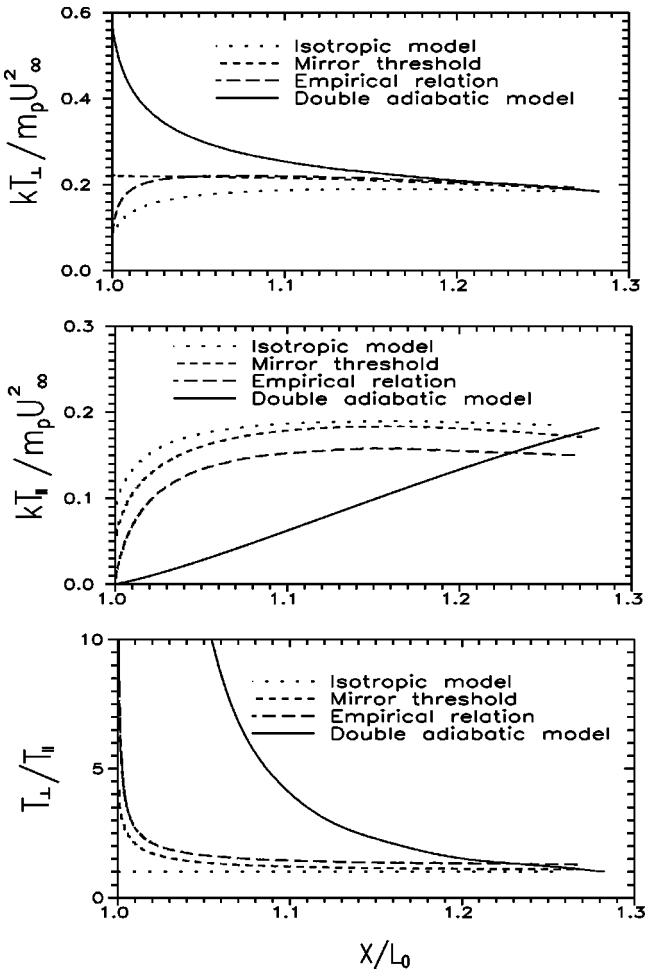

FIG. 3. Variation of temperatures and the perpendicular-to-parallel temperature ratio along the stagnation streamline.

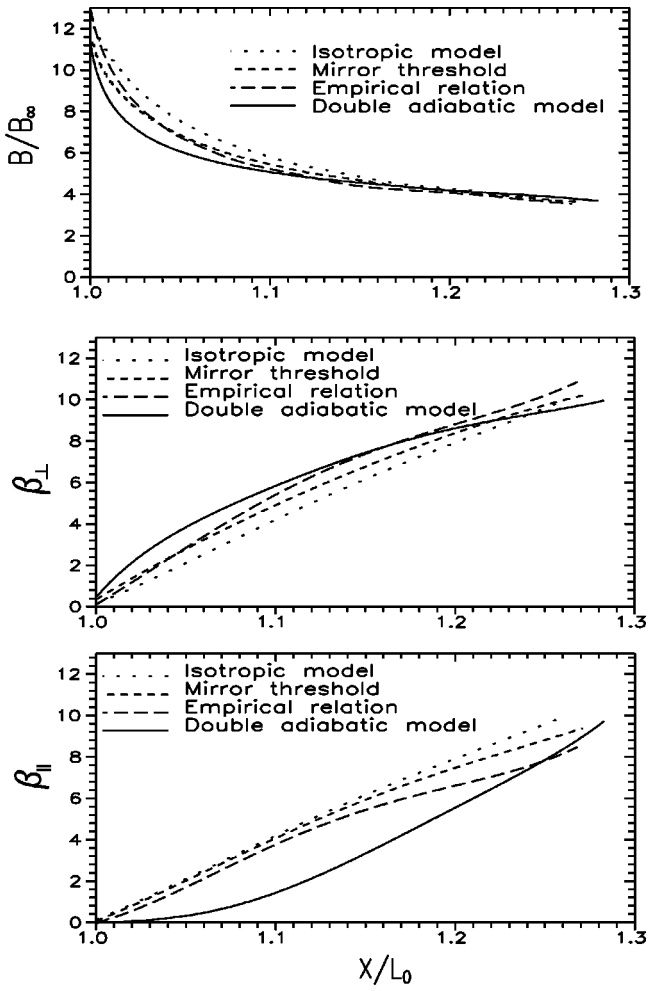

FIG. 4. Variation of the magnetic field strength and plasma betas along the stagnation streamline.

than the temperatures of the other models throughout most of the interval between the shock and the stagnation point. The other profiles have a shallow maxima before a systematic decrease toward the obstacle. All $T_\parallel$ profiles are bounded above by that of isotropy. The parallel temperature profile obtained in the mirror criterion model is the one closest to the isotropic case.

The last panel of Fig. 3 shows the variation of the temperature ratio $T_\perp/T_\parallel$. For the models with mirror and empirical criterions the temperature ratio starts close to 1 near the shock, and increases only very gradually across most of the interval between the shock and stagnation point. It then rises steeply towards the obstacle in a region where all other parameters show sharp gradients. The temperature ratio in the double-adiabatic model increases more strongly compared to the other models. This ratio is not bounded and exceeds substantially the values obtained in the other models throughout most of the part of the flow region between the shock and the obstacle.

Figure 4 shows the variation along the stagnation streamline of the magnetic field strength and the two β parameters related to perpendicular and parallel pressures. The magnetic field strength obtained in the double-adiabatic model increases more gradually across most of the region from the shock to the obstacle. It then rises rapidly near the obstacle. The magnetic field obtained in other models is larger throughout the region from the detached shock to the obstacle. But, the largest values correspond to the profile of the isotropic model. Thus, generally, anisotropy decreases the magnetic field strength between the shock and the obstacle.

The profiles of perpendicular plasma beta (second panel) related to the models with the mirror threshold and empirical criterion are very close to each other throughout most of the region between the detached shock and the obstacle. They are smaller than that for the double-adiabatic model, but larger than that for the isotropic case.

The profiles of the parallel plasma beta shown on the bottom panel are placed in reverse order to those of perpendicular beta. The lowest values are reached with the double-adiabatic ansatz, while the highest values correspond to isotropy. The parallel beta for the model with mirror criterion exceeds the parallel beta for the model with the empirical criterion throughout the trajectory between the detached shock and the obstacle. Generally, anisotropy increases the perpendicular beta and decreases the parallel beta.

Figure 5 shows the variation of the velocity component u_x along the stagnation streamline. There is little difference

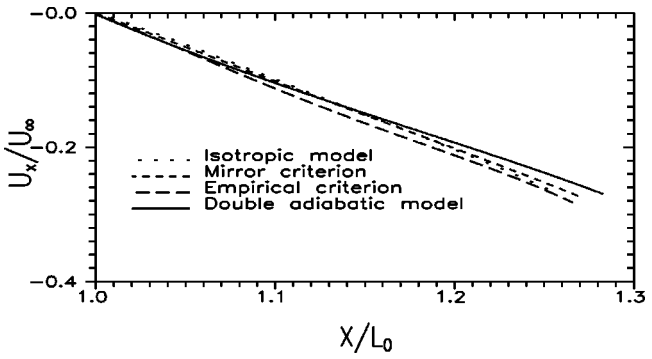

FIG. 5. Variation of the velocity along the stagnation streamline.

between the isotropic and anisotropic models using the mirror and empirical criterions. The velocity related to the double-adiabatic model has a smaller gradient than the others. But, a quasilinear decrease to zero is evident for all profiles.

Figure 6 shows the variations of the density, magnetic pressure, perpendicular and parallel pressures obtained in the model with the empirical criterion (5) for different Alfvén Mach numbers ($M_{A\infty}=5$, 10, 15, 20) under constant sonic Mach number, equal to 10. One can see from the behavior of magnetic field strength and plasma parameters near the obstacle for high Mach number the presence of a boundary layer, where the magnetic pressure exceeds the plasma pressure. The thickness of this layer for a high Alfvén Mach number is proportional to $\sim 1/M_{A\infty}^2$. Near the obstacle, the gradients of all parameters are sharper for a higher Alfvén Mach number. For an isotropic plasma, we refer to the work of Erkaev and Mezentsev.[4]

VI. DISCUSSION AND CONCLUSION

We study a 3D, ideal MHD flow model past a blunt obstacle, taking into account anisotropy of plasma temperature and pressure related to the magnetic field. We derived the magnetic string equations for an anisotropic plasma and applied them for the description of an ideal plasma frozen into magnetic field lines. These equations are just the ideal MHD equations expressed in material frozen-in coordinates under the assumptions concerning the behavior of the total pressure between the shock and the obstacle. In case the total pressure is a known function of the distance, the equations become a set of 2D hyperbolic equations.

Variations of temperature, plasma pressure, and beta parameter between the shock and the obstacle in the isotropic limit lie between variations of the corresponding quantities perpendicular (as upper bound) and parallel to the field. The difference between perpendicular and parallel temperatures is considerable, being on the order of the size of the parallel temperature. The difference between perpendicular and parallel pressures is also large, and the variation of the perpendicular pressure tracks that of the isotropic pressure. This is because the perpendicular plasma pressure plays a role similar to that of the isotropic pressure determining (together with the magnetic pressure) the normal momentum balance across the magnetosheath.

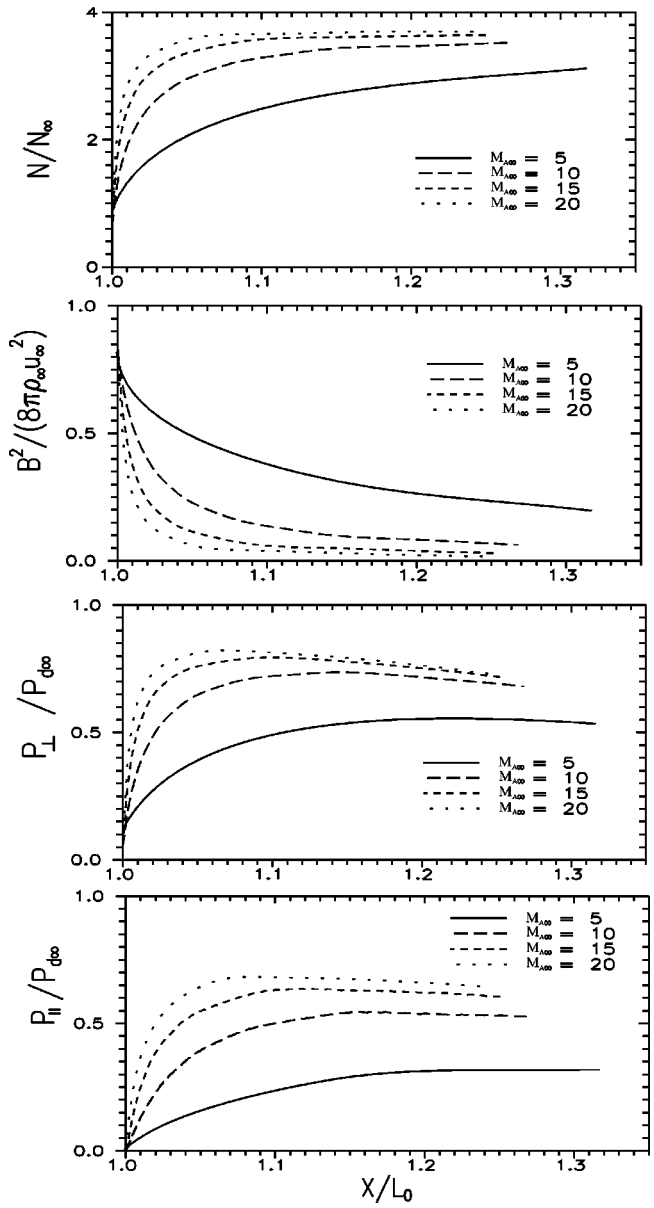

FIG. 6. Variation of density, magnetic pressure, and perpendicular and parallel plasma pressures obtained from the model with the empirical criterion for different Alfvén Mach numbers $M_{A\infty}=5$, 10, 15, 20 and a fixed sonic Mach number of 10.

In all anisotropic models, the perpendicular pressure is above and the parallel pressure is below the isotropic limit. The density is less than that in the isotropic limit throughout the region between the shock and the obstacle. Near the obstacle, this effect of additional decrease of density is much more pronounced because the stretching of the magnetic field is larger. From the frozen-in condition, we have $\rho s/B = \text{const}$, where s is distance between two fluid particles which belong to the same magnetic field line. This distance increases monotonically while fluid particles are moving towards the surface of the obstacle carrying the frozen-in magnetic field line. Thus, plasma density decreases according to the relation $\rho = \text{const}\, B/s$. Near the surface of the obstacle, the magnetic field strength is limited and the decrease of density is only affected by the increase of length s. Addi-

tional stretching (growth of parameter s) in the anisotropic case is caused by additional plasma acceleration along magnetic field lines. The expression for the flow acceleration in direction parallel to the magnetic field in dimensionless units can be obtained as follows:

$$w_{\parallel} = -\frac{1}{\rho}\mathbf{b}\cdot\nabla p_{\parallel} - \frac{1}{\rho}\frac{p_{\perp}-p_{\parallel}}{B}\mathbf{b}\cdot\nabla B, \tag{30}$$

where **b** is a unit vector along **B**. Additional acceleration is caused by the second term (the ''mirror force,'' as pointed out by Denton and Lyon[8]), which is positive.

The Alfvén Mach number, $M_{A\infty}$, is a measure of the strength of ''MHD effects,'' and as this parameter is lowered, the magnetic forces exert an increasingly larger influence on the flow. The increase of the Alfvén Mach number brings about an increase of gradients of plasma parameters near the obstacle. Substantial decrease of plasma density and pileup of magnetic field strength takes place in the boundary layer adjacent to the obstacle. The thickness of this layer is inversely proportional to the square of the Alfvén Mach number.

An ideal MHD model with anisotropic pressure has wide applications for the solar wind flow around magnetospheres of planets and magnetic clouds. In particular, density depletion and magnetic strength rise calculated in our model using the empirical criterion, are consistent with those obtained by a superposed epoch analysis[23] for the solar wind flow around the earth's magnetosphere.

ACKNOWLEDGMENTS

Part of this work was done while N.V.E. and C.J.F. were on a research visit to the Space Research Institute of the Austrian Academy of Sciences in Graz.

This work is supported by the INTAS-ESA Project No. 99-01277, by Grant No 98-05-65290 from the Russian Foundation of Basic Research, by Grant No. 97-0-13.0-71 from the Russian Ministry of Education, by the Austrian ''Fonds zur Föderung der Wissenschaftlichen Forschung'' under Project No. P12761-TPH, and by NASA Grant No. NAG5-2834.

[1] J. R. Spreiter, A. L. Summers, and A. Y. Alskne, Planet. Space Sci. **14**, 223 (1966).
[2] B. J. Zwan and R. A. Wolf, J. Geophys. Res. **81**, 1636 (1976).
[3] N. V. Erkaev, Geomagn. Aeron. **28**, 529 (1988).
[4] N. V. Erkaev and A. V. Mezentsev, in *Solar Wind-Magnetosphere Interaction*, edited by M. F. Heyn, H. K. Biernat, V. S. Semenov, and R. P. Rijnbeek (Österreichische Akademie der Wissenschaften, Vienna, 1992), p. 43.
[5] N. V. Erkaev, C. J. Farrugia, and H. K. Biernat, in *Polar Cap Boundary Phenomena*, edited by J. Moen *et al.* (Kluwer Academic, Dordrecht, 1998), p. 27.
[6] C. C. Wu, Geophys. Res. Lett. **19**, 87 (1992).
[7] I. H. Cairns and J. V. Lyon, J. Geophys. Res. **100**, 17173 (1995).
[8] R. E. Denton and J. G. Lyon, Geophys. Res. Lett. **23**, 2891 (1996).
[9] N. V. Erkaev, C. J. Farrugia, and H. K. Biernat, J. Geophys. Res. **104**, 6877 (1999).
[10] G. F. Chew, M. L. Goldberger, and F. E. Low, Proc. R. Soc. London **A236**, 112 (1956).
[11] W. B. Thompson, *An Introduction to Plasma Physics* (Pergamon, New York, 1964).
[12] M. Tajiri, J. Phys. Soc. Jpn. **22**(6), 1482 (1967).
[13] S. P. Gary, M. D. Montgomery, W. C. Feldman, and D. W. Forslund, J. Geophys. Res. **81**, 1241 (1976).
[14] L. N. Hau, T. D. Phan, B. U. Sonnerup, and G. Paschmann, Geophys. Res. Lett. **20**, 2255 (1993).
[15] S. P. Gary, B. J. Anderson, R. E. Denton, S. A. Fuselier, and M. E. McKean, Phys. Plasmas **1**, 1676 (1994).
[16] R. E. Denton, B. J. Anderson, S. P Gary, and S. A. Fuselier, J. Geophys. Res. **99**, 11225 (1994).
[17] S. P. Gary, S. A. Fuselier, and B. J. Anderson, J. Geophys. Res. **98**, 1481 (1993).
[18] H. Weitzner, in *Handbook of Plasma Physics*, edited by A. A. Galeev and R. N. Sudan (North-Holland, Amsterdam, 1983), Vol. 1, p. 201.
[19] M. I. Pudovkin and V. S. Semenov, Ann. Geophys. **33**, 429 (1977).
[20] N. V. Erkaev, C. J. Farrugia, and H. K. Biernat, J. Geophys. Res. **101**, 10665 (1996).
[21] H. K. Biernat, N. V. Erkaev, and C. J. Farrugia, J. Geophys. Res. **104**, 12617 (1999).
[22] C. J. Farrugia, N. V. Erkaev, H. K. Biernat, and L. F. Burlaga, J. Geophys. Res. **100**, 19245 (1995).
[23] T. D. Phan, G. Paschmann, W. Baumjohann, N. Sckopke, and H. Luehr, J. Geophys. Res. **99**, 121 (1994).